Wave-packet dynamical analysis of ultracold scattering in cylindrical waveguides

Vladimir S. Melezhik,[1] J. I. Kim,[2] and Peter Schmelcher[3,4]
[1]*Bogoliubov Laboratory of Theoretical Physics, Joint Institute for Nuclear Research, Dubna, Moscow Region 141980, Russian Federation*
[2]*Departamento de Ciências Exatas e da Terra, Universidade Federal de São Paulo, Rua Professor Artur Riedel 275, CEP 09972-270, Diadema, São Paulo, Brazil*
[3]*Physikalisches Institut, Universität Heidelberg, Philosophenweg 12, 62120 Heidelberg, Germany*
[4]*Theoretische Chemie, Institut für Physikalische Chemie, Universität Heidelberg, Im Neuenheimer Feld 229, 69120 Heidelberg, Germany*
(Received 3 August 2007; published 13 November 2007)

A wave-packet propagation method is developed and applied to investigate the quantum dynamics of scattering processes of identical and distinguishable atoms in harmonic waveguides. The quantum dynamics of the confinement-induced resonances (CIRs) for ultracold collisions of identical particles, *s*-wave CIRs for bosons and *p*-wave CIRs for fermions, is explored in detail. Our multigrid approach allows us to fully take into account the coupling between the center-of-mass (c.m.) and relative motions in the case of distinguishable atoms. The latter includes, in particular, *s*- and *p*-partial-wave mixing, caused by the confining trap, which acts differently on the different atomic species. Specifically, we explore in detail the recently discovered [J. I. Kim, V. S. Melezhik, and P. Schmelcher, Phys. Rev. Lett. **97**, 193203 (2006)] dual CIR, which is based on a destructive interference mechanism leading to complete transmission in the waveguide, although the corresponding scattering in free space exhibits strong *s*- and *p*-wave scattering.

DOI: 10.1103/PhysRevA.76.053611 PACS number(s): 03.75.Be, 34.10.+x, 34.50.−s

I. INTRODUCTION

Ultracold atomic collisions in tight optical and magnetic traps represent a rapidly developing field of research with a rich impact on ultracold many-body systems, whether of bosonic, fermionic, or mixed nature. By employing optical lattices [1] or atomic chips [2], it is nowadays possible to confine an atomic system in the nanometer regime. One of the seminal contributions in the theory of binary atomic collisions in the presence of confinement was provided by Olshanii [3]. In this work, cold atom-atom scattering under a transverse harmonic confinement was reduced to a quasi-one-dimensional (1D) scattering with the *s*-wave zero-range pseudopotential $g_{1D}\delta(z)$, defined by the effective 1D coupling constant g_{1D}. This leads to the prediction of a so-called confinement-induced resonance (CIR) for the ultracold atom-atom scattering process. The CIR is accompanied by total atom-atom reflection, thereby creating a gas of impenetrable bosons. The properties of the resulting 1D system of fermionized bosons—the Tonks-Girardeau gas [4]—have been theoretically studied in detail [5], stimulated by its recent experimental verification [6]. Part of the attractiveness of the CIR phenomenon stems from the mere fact that it provides us with a handle to tune the strength of the interacting atoms, and, of course, varying this interaction leads to crossovers in the qualitative behavior of the corresponding many-body systems. Experimental evidence for the CIR for fermions has been obtained recently in optical lattices [7]. So far, the quasi-1D scattering under transverse confinement has been analyzed mostly either in the pure *s*-wave approximation, when the odd part f_u of the scattering amplitude $f=f_g+f_u$ is equal to zero, $f_u=0$ (see, for example, [3,8,9]), or in the pure *p*-wave approximation [10], when the even part is equal to zero, $f_g=0$. Aiming beyond the pseudopotential approach, a more general analytical treatment that can include all partial waves and their couplings among each other was first given in Ref. [11], where, however, effects of the center-of-mass (c.m.) were not taken into account. The framework of the approximation $f_u=0$ was also assumed in Ref. [12], where effects due to the center-of-mass nonseparability for two distinguishable particles scattering in a cylindrical waveguide were analyzed within the *s*-wave zero-range pseudopotential approach and in the zero-energy limit.

In the present work, we employ a wave-packet propagation method in order to explore the scattering of two distinguishable particles at low collision energies in a transverse harmonic trap forming a waveguide. Here we are not restricted to only even or only odd scattering amplitudes, as is the case for identical particles. Our computational scheme also allows us to verify the well-known CIR effects for identical particles but now from a unified quantum-dynamical point of view: the *s*-wave CIR for bosons [3,8,9] and *p*-wave CIR for fermions [10]. The analysis for the general case of two distinguishable particles demands a detailed study of effects due to the coupling of the c.m. to the relative motion of the atoms, including the resulting mixing of *s* and *p* partial waves. Furthermore, we provide a detailed quantitative analysis of the dual CIR, predicted originally in Refs. [13,14] for the case of simultaneous near-resonant *s*- and *p*-wave contributions for 3D scattering in free space.

The content of the paper is as follows. In Sec. II we formulate the problem. Here we also introduce a unitary transformation of the initial 5D Hamiltonian which reduces it to a 4D one. The computational scheme is presented in Sec. III, which contains a discussion of specific computational aspects essential to the problem. In Sec. IV the modeling of the interatomic interaction for scattering in 3D free space is considered. In Sec. V we present and discuss the results of our investigations for two cases: first, the one-component atom-

atom scattering in a harmonic cylindrical waveguide permitting the separation of the c.m. and, second, a two-component gas in a harmonic waveguide exhibiting c.m. nonseparability. We analyze effects due to the rich spectral structure of the interatomic interaction and due to the coupling of the c.m. and relative motions induced by the trap confinement. We demonstrate that comparable contributions of s- and p-wave resonant behavior in the free-space two-body scattering process can lead in cylindrical confinement to the so-called dual CIR, for which one observes total transmission, i.e., suppression of the effective two-body interaction in the waveguide. This is in contrast to the total reflection observed in the CIR cases of pure resonant s-wave [3] or pure resonant p-wave [10] scattering. The brief conclusions are provided in Sec. VI.

II. HAMILTONIAN AND TRANSFORMATIONS

Let us consider two different interacting atoms with masses m_1 and m_2 under the action of a transverse 2D confining trap represented by harmonic potentials with different frequencies ω_1 and ω_2. Since the confinement is only two dimensional, this corresponds to a scattering process in a waveguide. We will solve the resulting six-dimensional problem in the space $(\boldsymbol{R},\boldsymbol{r})$ of the center-of-mass $\boldsymbol{R}=(Z,\boldsymbol{\rho}_{\boldsymbol{R}})=(Z,\rho_R,\phi_R)$ and relative $\boldsymbol{r}=(z,\boldsymbol{\rho})=(z,\rho,\phi)\leftrightarrow(r,\theta,\phi)$ coordinate variables. Due to the cylindrical symmetry of the confinement, the motion in the Z direction separates, and the problem reduces to a 5D time-dependent Schrödinger equation ($\hbar=1$)

$$i\frac{\partial}{\partial t}\psi'(\boldsymbol{\rho}_{\boldsymbol{R}},\boldsymbol{r},t)=H'(\boldsymbol{\rho}_{\boldsymbol{R}},\boldsymbol{r})\psi'(\boldsymbol{\rho}_{\boldsymbol{R}},\boldsymbol{r},t), \tag{1}$$

which we will integrate in time from $t=0$ to the asymptotic region $t\to+\infty$ with the following initial condition:

$$\psi'(\boldsymbol{\rho}_{\boldsymbol{R}},\boldsymbol{r},t=0)=N\varphi_0'(\rho_R,\phi_R,\rho,\phi)\exp\left(-\frac{(z-z_0)^2}{2a_z^2}\right)\exp(ikz), \tag{2}$$

representing a 5D wave packet of two atoms with a maximum at $z=z_0\to-\infty$, $k>0$ and with the relative interatomic velocity $v_0=k/\mu=\sqrt{2\varepsilon/\mu}$. The asymptotic behavior reads $\psi'(\boldsymbol{\rho}_{\boldsymbol{R}},\boldsymbol{r},t=0)\to Nr\sqrt{\rho_R}$ for $\rho_R\to 0$, $r\to 0$. N is the normalization constant with the volume element being $d\rho_R dr\sin\theta\, d\theta\, d\phi$. The function φ_0' represents the ground state of two different noninteracting atoms in the harmonic confinement potential:

$$\varphi_0'(\rho_R,\phi_R,\rho,\phi)=r\sqrt{\rho_R}\exp\left[-\frac{\rho_R^2}{2}\left(\frac{1}{a_1^2}+\frac{1}{a_2^2}\right)-\frac{(\mu\rho)^2}{2}\left(\frac{1}{(m_1a_1)^2}+\frac{1}{(m_2a_2)^2}\right)-\frac{\rho\rho_R}{M}\left(\frac{m_2}{a_1^2}-\frac{m_1}{a_2^2}\right)\cos(\phi-\phi_R)\right]. \tag{3}$$

The Hamiltonian takes on the appearance

$$H'(\boldsymbol{\rho}_{\boldsymbol{R}},\boldsymbol{r})=-\frac{1}{2M}\left(\frac{\partial^2}{\partial\rho_R^2}+\frac{1}{4\rho_R^2}\right)-\frac{1}{2M\rho_R^2}\frac{\partial^2}{\partial\phi_R^2}+\frac{1}{2}(m_1\omega_1^2+m_2\omega_2^2)\rho_R^2-\frac{1}{2\mu}\frac{\partial^2}{\partial r^2}+\frac{L^2(\theta,\phi)}{2\mu r^2}+\frac{\mu^2}{2}\left(\frac{\omega_1^2}{m_1}+\frac{\omega_2^2}{m_2}\right)\rho^2+\mu(\omega_1^2-\omega_2^2)\times\rho\rho_R\cos(\phi-\phi_R)+V(r); \tag{4}$$

here the definitions $a_1=1/\sqrt{m_1\omega_1}$, $a_2=1/\sqrt{m_2\omega_1}$ have been introduced. $M=m_1+m_2$ and $\mu=m_1m_2/M$ are the total and reduced masses of the atoms, respectively. The parameter a_z defines the width of the initial wave packet in the z direction, and the interatomic potential $V(r)$ depends exclusively on the distance $r=|\boldsymbol{r}_2-\boldsymbol{r}_1|$ between the atoms.

Following Ref. [15], we remove the dependence on the angular variable ϕ_R of the c.m. by the unitary rotating-frame transformation

$$U=\exp(i\phi_R L_z) \tag{5}$$

with $L_z=(1/i)(\partial/\partial\phi)$. This replaces $\phi-\phi_R$ by ϕ and $\partial/\partial\phi_R$ by $\partial/\partial\phi_R-\partial/\partial\phi$ in the above Hamiltonian, leading to the new Hamiltonian $UH'U^+=H$. The wave packet transforms accordingly, $U\psi'=\psi$. The resulting elimination of the degree of freedom ϕ_R is possible due to the conservation of the total angular momentum (L_z+L_Z), i.e., it commutes with H'. We are therefore left with the 4D time-dependent Schrödinger equation

$$i\frac{\partial}{\partial t}\psi(\rho_R,\boldsymbol{r},t)=[H^{(0)}(\rho_R,\boldsymbol{r})+V(r)]\psi(\rho_R,\boldsymbol{r},t), \tag{6}$$

where the wave packet $\psi(\rho_R,\boldsymbol{r},t)$ represents the time evolution of the relative and c.m. motions, and

$$H^{(0)}(\rho_R,\boldsymbol{r})=-\frac{1}{2M}\left(\frac{\partial^2}{\partial\rho_R^2}+\frac{1}{4\rho_R^2}\right)-\frac{1}{2M\rho_R^2}\left(\frac{\partial}{\partial\phi_R}-\frac{\partial}{\partial\phi}\right)^2+\frac{1}{2}(m_1\omega_1^2+m_2\omega_2^2)\rho_R^2-\frac{1}{2\mu}\frac{\partial^2}{\partial r^2}+\frac{L^2(\theta,\phi)}{2\mu r^2}+\frac{\mu^2}{2}\left(\frac{\omega_1^2}{m_1}+\frac{\omega_2^2}{m_2}\right)\rho^2+\mu(\omega_1^2-\omega_2^2)\rho\rho_R\cos\phi \tag{7}$$

is the Hamiltonian of two noninteracting different atoms moving in the trap. Our investigations focus on the case $M_{\phi_R}=0$, the latter being the quantum number corresponding to $(1/i)(\partial/\partial\phi_R)$. Note that for the case $\omega_1=\omega_2$ the last term of $H^{(0)}$ vanishes, and consequently the c.m. and relative motions separate. For this special case, the scattering problem reduces to a two-dimensional one.

III. WAVE-PACKET DYNAMICAL TOOLS AND COMPUTATIONAL METHOD

Our approach to solving the above-defined Schrödinger problem was originally developed in Refs. [16] for the treat-

ment of bound-continuum transitions of hydrogenlike ions in a laser field. In subsequent works, it has been successfully applied to a variety of different atomic and nuclear problems [16]. It has therefore proven to be a very efficient and flexible approach for studies of quantum dynamics in three dimensions. Here we extend this computational scheme in order to describe continuum-continuum transitions in the four-dimensional space spanned by $(\rho_R, r, \theta, \phi)$, which is a challenging task. Let us provide the main features of our approach.

A. General scheme

The wave packet starts propagating at $t=0$ with the initial state

$$\psi(\rho_R, \boldsymbol{r}, t=0) = N\varphi_0(\rho_R, \rho, \phi)\exp\left(-\frac{(z-z_0)^2}{2a_z^2}\right)\exp(ikz)$$
$$= N\varphi_0(\rho_R, \rho, \phi)\chi(z-z_0)\exp(ikz), \tag{8}$$

representing two different noninteracting atoms in the transversal ground state of the waveguide. Initially we choose z_0 to be far from the origin $z=0$, i.e., interaction effects can be neglected. The wave packet moves with the positive relative interatomic velocity $v_0=k/\mu=\sqrt{2\varepsilon/\mu}$ and has the initial longitudinal dispersion $D_z(t=0)=a_z^2/2$ given by the parameter a_z. In the course of the collision process the wave packet splits up into two parts moving in opposite directions $z \to \pm\infty$. Asymptotically, we encounter the following behavior [3,8,11]:

$$|\psi(t \to +\infty)\rangle \begin{cases} \underset{z\to+\infty}{\to} |\psi(t)^+\rangle = [1+f^+(k)]N\varphi_0(\rho_R, \rho, \phi)\tilde{\chi}(z-(z_0+vt))\exp(ikz), \\ \underset{z\to-\infty}{\to} |\psi(t)^-\rangle = f^-(k)N\varphi_0(\rho_R, \rho, \phi)\tilde{\chi}(-z-(z_0+vt))\exp(-ikz), \end{cases} \tag{9}$$

where

$$f^{\pm}(k) = \mathrm{Re}[f^{\pm}(k)] + i\ \mathrm{Im}[f^{\pm}(k)]$$

are the atom-atom forward and backward scattering amplitudes in the presence of the external confining potential. In the special case $\omega_1=\omega_2$ of interacting atoms experiencing the same harmonic trap, the even and odd partial waves are decoupled and the forward-backward amplitudes $f^{\pm}$ can be written as a sum

$$f^{\pm}(k) = f_g(k) \pm f_u(k)$$

of even-odd (gerade-ungerade) scattering amplitudes f_g and f_u. $\tilde{\chi}$ describes the motion and in particular the spreading of the initial Gaussian wave packet in the z direction. In the absence of scattering, it propagates according to

$$\tilde{\chi}(z-(z_0+vt)) \to \left(\frac{D_z(t)}{a_z^2}\right)^{-1/4}\exp\left[-\frac{[z-(z_0+vt)]^2}{4D_z(t)}\left(1-i\frac{t}{\mu a_z^2}\right)+i\varepsilon t\right],$$

where $D_z(t)=(a_z^2/2)[1+t^2/(\mu^2 a_z^4)]$. Employing the solution to the scattering problem in the absence of atom-atom interaction $[V(r)=0]$ at large times $t\to+\infty$ as

$$|\psi^{(0)}(t \to +\infty)\rangle \times \begin{cases} \underset{z\to+\infty}{\to} |\psi^{(0)+}\rangle = N\varphi_0(\rho_R, \rho, \phi)\tilde{\chi}(z-(z_0+vt))\exp(ikz), \\ \underset{z\to-\infty}{\to} |\psi^{(0)-}\rangle = 0, \end{cases} \tag{10}$$

and additionally the fact that our computational scheme (see below) is unitary, i.e., conserves the norm during propagation $\langle\psi^{(0)}(t)|\psi^{(0)}(t)\rangle=\langle\psi(t)|\psi(t)\rangle=1$, we can extract the forward scattering amplitude as follows:

$$\langle\psi^{(0)}(t)|\psi(t)\rangle \underset{t\to+\infty}{\to} [1+f^+(k)], \tag{11}$$

which is valid in the asymptotic region $t\to+\infty$. The amplitude $f^+(k)$ is a fundamental scattering parameter and its knowledge provides a complete description of the quasi-1D scattering in the waveguide (note that, for the case of energies above the first transversal excited state, which are not considered here, inelastic multichannel processes are possible and the scattering amplitude has to be generalized correspondingly). Exploiting current conservation, one can represent the transmission T and reflection R coefficients as follows [11]:

$$T(k) = |1+f^+(k)|^2, \quad R(k) = 1-|1+f^+(k)|^2.$$

The above expression for the reflection coefficient $R(k)$ holds for elastic scattering processes. In the case of inelastic scattering, current conservation is in general violated, and one has to replace the reflection coefficient by the expression $R=|f^-(k)|^2$.

For the special case $f^+=f^-$, valid in the s-wave zero-range pseudopotential approach when $f_u=0$, the quasi-1D coupling constant

$$g_{1D} = \lim_{k\to0}\frac{k}{\mu}\frac{\mathrm{Re}[f_g(k)]}{\mathrm{Im}[f_g(k)]} = \lim_{k\to0}\frac{k}{\mu}\frac{\mathrm{Re}[f^+(k)]}{\mathrm{Im}[f^+(k)]} \tag{12}$$

has been introduced, together with the quasi-1D scattering length a_{1D}, in Refs. [3,8,9],

$$g_{1D} = -\frac{1}{\mu a_{1D}}.$$

It has also been shown [3,9] that in the zero-energy limit the scattering under an isotropic 2D harmonic confinement can be parametrized by a single scattering parameter (for $f_u=0$), e.g., a_{1D} or g_{1D}. The expression (12) holds also for the parameter $k^2 g_{1D}^{map}$ introduced in Ref. [10] for the case $f_g=0$ of two spin-polarized fermions interacting via pure p-wave scattering [here it needs the replacement $\mathrm{Re}(f_g) \rightleftharpoons \mathrm{Im}(f_u)$ in Eq. (12)].

The quasi-1D effective coupling constants g_{1D} and g_{1D}^{map} can be extracted from the amplitude f^+ by employing the low-energy $k \to 0$ and asymptotic limit according to Eqs. (12) and (11), respectively. This holds in particular for the case that the interatomic interaction $\hat{V}(r)$ scatters only even, $\hat{V}(r)=V(r)\delta_{l,2l'}$, or only odd, $\hat{V}(r)=V(r)\delta_{l,2l'+1}$, waves l ($l'=0,1,2,\ldots$), which corresponds to the situation $\omega_1=\omega_2$, i.e., no gerade-ungerade mixing term $\mu(\omega_1^2-\omega_2^2)\rho\rho_R \cos\phi$ is present in the Hamiltonian (7). Indeed, numerically solving the Schrödinger equation (6) with the interaction operator $\hat{V}(r)=V(r)\delta_{l,2l'}$, acting exclusively on even partial waves, instead of employing the potential $V(r)$, acting on all partial waves, permits us to extract $f_g(k)$ directly from the calculated forward scattering amplitude Eq. (11) if $\omega_1=\omega_2$. In this case there is no scattering of the odd waves, $f_u(k)=0$, and thus $f^+(k)=f_g(k)$. In the zero-energy limit $\varepsilon \to 0$, such a procedure models the pure s-wave approximation considered earlier [3,8,9]. In our scheme, modeling the pure p-wave approximation used in [10] works analogously to the above procedure with $\hat{V}(r)=V(r)\delta_{l,2l'+1}$.

In the case $\omega_1 \neq \omega_2$ of gerade-ungerade partial-wave mixing, it is not possible to parametrize the scattering process in the low-energy limit with a single scattering parameter such as a_{1D} or g_{1D}. The reason for this is that, even in the asymptotic region $r \to \infty$, the term $\sim\mu(\omega_1^2-\omega_2^2)\rho_R\rho\cos\phi \sim \mu(\omega_1^2-\omega_2^2)\rho_R r \sin\theta\cos\phi$ induces a strong gerade-ungerade partial-wave coupling which modifies the partial scattering amplitude $f_u(k)$ to possess the same dependence on k as $f_g(k)$ for $k \to 0$ (see, e.g., [17] and references therein). Even in the zero-energy limit we cannot neglect either the even or the odd partial waves in any case if $\omega_1 \neq \omega_2$. As a consequence, pure s-wave scattering does not occur for $\omega_1 \neq \omega_2$, and the effective 1D s-wave pseudopotential approach $g_{1D}\delta(z)$ cannot be considered as an adequate description of the scattering process.

Following the computational scheme developed in Refs. [16], we treat the angular part of the scattering process without using a partial-wave decomposition. Instead of spherical harmonics we use a two-dimensional angular basis, constructed from the eigenfunctions of the angular operator $L^2(\theta,\phi)$ and defined on the angular grid (θ_j,ϕ_j) in the spirit of the discrete-variable representation (DVR) [18] and/or the Lagrange-mesh method [19]. This yields a diagonal representation for the angular part of the interaction between the atoms and the harmonic trap in the Hamiltonian $H^{(0)} \times(\rho_R,r,\theta_j,\phi_j,t)$. As a consequence, we arrive at a set of radial equations of motion coupled exclusively via the nondiagonal angular part of the kinetic energy operator. These equations are solved using a component-by-component split-operator method, which permits a fast diagonalization of the nondiagonal part [16]. Concerning the discretization with respect to the radial variables r and ρ_R, a sixth-order (seven-point) finite-difference approximation on a quasiuniform grid is used. This scheme has the same order of accuracy as the conventional Crank-Nicholson algorithm. It allows a full 4D quantum treatment of the atomic collision process.

B. Discretization of the angular subspace

We are seeking for the time-dependent solution $\psi(\rho_R,\boldsymbol{r},t)$, employing the variables $(\rho_R,r,\Omega)=(\rho_R,r,\theta,\phi)$ according to the expansion [16]

$$\psi(\rho_R,r,\Omega,t) = \sum_j^N f_j(\Omega)\psi_j(\rho_R,r,t) \tag{13}$$

with respect to the two-dimensional basis

$$f_j(\Omega) = \sum_\nu^N Y_\nu(\Omega)(Y^{-1})_{\nu j} \tag{14}$$

associated with a mesh $\Omega_j=(\theta_{j_\theta},\phi_{j_\phi})$. For the θ variable, the N_θ mesh points θ_{j_θ} correspond to the zeros of the Legendre polynomial $P_{N_\theta}(\cos\theta_{j_\theta})=0$. For the ϕ variable, the N_ϕ mesh points are chosen as $\phi_{j_\phi}=\pi(2j_\phi-1)/N_\phi$. The total number $N=N_\theta N_\phi$ of grid points $\Omega_j=(\theta_{j_\theta},\phi_{j_\phi})$ is equal to the number of basis functions in the expansion (13) and the number of terms in the definition (14), where the symbol ν represents the twofold index $\{l,m\}$ and the sum over ν is equivalent to the double sum

$$\sum_{\nu=1}^{N} = \sum_{m=-(N_\phi-1)/2}^{(N_\phi-1)/2} \sum_{l=|m|}^{|m|+N_\theta-1}. \tag{15}$$

The l and m indices show the number of zeros over the θ and ϕ variables of the polynomials $Y_\nu(\Omega)$ which we specify in the next paragraph. Due to the definition (15) the values N_ϕ may be chosen only odd. N_θ can take on arbitrary values. The coefficients $(Y^{-1})_{\nu j}$ in the definition (14) are the elements of the $N\times N$ matrix Y^{-1} inverse to the matrix given by the values $Y_{j\nu}=Y_\nu(\Omega_j)$ of the polynomials $Y_\nu(\Omega)$ at the grid points Ω_j. It is clear that $f_j(\Omega_{j'})=\delta_{jj'}$ with this definition [i.e., the basis (14) belongs to the class of Lagrange functions [19]] and the coefficients $\psi_j(\rho_R,r,t)$ in the expansion (13) are the values of the required solution $\psi(\rho_R,\boldsymbol{r},t)$ at the points of the angular grid $\psi_j(\rho_R,r,t)=\psi(\rho_R,r,\Omega_j,t)$.

The polynomials $Y_\nu(\Omega)$ in Eq. (14) are chosen as

$$Y_\nu(\Omega) = Y_{lm}(\Omega) = e^{im\phi}\sum_{l'} C_l^{l'} P_{l'}^m(\theta), \tag{16}$$

where $C_l^{l'}=\delta_{ll'}$ holds in general, and thus $Y_\nu(\Omega)$ coincides with the usual spherical harmonic with a few possible exceptions for large values of ν such that we obtain the orthogonality relation

$$\int Y_\nu^*(\Omega) Y_{\nu'}(\Omega) d\Omega \approx \sum_j \lambda_j Y_{\nu j}^* Y_{\nu' j} = \delta_{\nu\nu'} \tag{17}$$

for all ν and $\nu' \leq N$. Here, the N weights λ_j are the standard Gauss-Legendre weights multiplied by $2\pi/N_\phi$. For most ν and ν', the above relation is automatically satisfied because the basis functions $Y_\nu(\Omega)$ are orthogonal and the Gaussian quadrature is exact. For these ν we have $C_l^{l'} = \delta_{ll'}$ in Eq. (16). However, in a few cases involving the highest l values, some polynomials Y_l^m have to be orthogonalized in the sense of the Gaussian quadrature ($C_l^{l'} \neq \delta_{ll'}$ for these specific values of l). With this choice, the matrix $S_{j\nu} = \lambda_j^{1/2} Y_{j\nu}$ is orthogonal.

The values of the wave function $\psi(\rho_R, \boldsymbol{r}, t)$ at the grid points of the angular space $\psi(\rho_R, r, \Omega_j, t) = \psi_j(\rho_R, r, t)$ are utilized in the spirit of the discrete-variable representation [18] or Lagrange-mesh methods [19]. This procedure drastically simplifies the calculations [16] as compared to the usual partial-wave analysis.

C. Computational scheme

It is an attractive feature of our two-dimensional DVR (14) that for the grid representation $f_j(\Omega)$ the only nondiagonal part of the Hamiltonian in Eq. (6) is the angular part of the kinetic energy operator [see Eq. (7)],

$$\left(\frac{1}{2\mu r^2} L^2(\theta,\phi) - \frac{1}{2M\rho_R^2}\frac{\partial^2}{\partial\phi^2}\right) \sum_\nu^N Y_\nu(\Omega)(Y^{-1})_{\nu j'}|_{\Omega=\Omega_j}$$
$$= \sum_\nu^N Y_{j\nu}\left(\frac{l(l+1)}{2\mu r^2} + \frac{m^2}{2M\rho_R^2}\right)(Y^{-1})_{\nu j'},$$

which can be diagonalized by the simple unitary transformation $S_{j\nu} = \lambda_j^{1/2} Y_{j\nu}$ [16]. This property has been exploited for developing an efficient algorithm with a computational time scaling according to the number $N = N_\theta N_\phi$ of unknowns in the system of Eqs. (6) [16]. As in previous works (see Ref. [16] and references therein), we apply here for the propagation $\psi(\rho_R, r, \Omega_j, t_n) \to \psi(\rho_R, r, \Omega_j, t_{n+1})$ in time $t_n \to t_{n+1} = t_n + \Delta t$ the component-by-component split-operator method [20]. The Hamiltonian (7) permits a splitting into the following three parts:

$$H_{jj'}^{(0)}(\rho_R, r) = h_{jj'}^{(0)}(\rho_R) + h_{jj'}^{(1)}(r) + W_j(\rho_R, \rho)\delta_{jj'}, \tag{18}$$

where

$$h_{jj'}^{(0)}(\rho_R) = -\frac{1}{2M}\left(\frac{\partial^2}{\partial\rho_R^2} + \frac{1}{4\rho_R^2}\right)$$
$$+ \frac{1}{2M\rho_R^2\sqrt{\lambda_j\lambda_{j'}}} \sum_\nu^N (Y^{-1})_{\nu j} m^2 (Y^{-1})_{\nu j'},$$

$$h_{jj'}^{(1)}(r) = -\frac{1}{2\mu}\frac{\partial^2}{\partial r^2} - \frac{1}{2\mu r^2\sqrt{\lambda_j\lambda_{j'}}} \sum_\nu^N (Y^{-1})_{\nu j} l(l+1)(Y^{-1})_{\nu j'},$$

$$W_j(\rho_R, \rho) = \frac{1}{2}(m_1\omega_1^2 + m_2\omega_2^2)\rho_R^2 + \frac{\mu^2}{2}\left(\frac{\omega_1^2}{m_1} + \frac{\omega_2^2}{m_2}\right)\rho^2$$
$$+ \mu(\omega_1^2 - \omega_2^2)\rho\rho_R \cos\phi_j.$$

Subsequently, we can approximate the time step $\psi(\rho_R, r, \Omega_j, t_n) \to \psi(\rho_R, r, \Omega_j, t_{n+1})$ where $t_n \to t_{n+1} = t_n + \Delta t$ according to

$$\psi(t_n + \Delta t) = \exp\left(-\frac{i}{2}\Delta t\hat{W}\right)\exp[-i\Delta t(\hat{h}^{(1)} + V)]$$
$$\times \exp(-i\Delta t\hat{h}^{(0)})\exp\left(-\frac{i}{2}\Delta t\hat{W}\right)\psi(t_n) + O(\Delta t^3). \tag{19}$$

The time evolution proceeds as follows. For the first and the last steps, according to the relation (19), we write the function ψ and the operators $\exp(-i\Delta t\hat{W}/2)$ in our two-dimensional DVR (14) on the grid $\{\Omega_j\} = \{\theta_{j_\theta}, \phi_{j_\phi}\}$. Since the potential $W_j(\rho_R, \rho)$ is diagonal in this representation, the first and last steps represent simple multiplications of the diagonal matrices $\exp[-(i/2)\Delta t W_j(\rho_R, \rho)]$. Two intermediate steps in (19) depending on $\hat{h}^{(0)}$ and $\hat{h}^{(1)}$ are treated in the basis Y_ν (16) where the matrix operators $\hat{h}^{(0)}(\rho_R)$ and $\hat{h}^{(1)}(r)$ are diagonal with respect to the indices m and l. For that we approximate the exponential operators according to

$$\exp(-i\Delta t\hat{A}) \approx \left(1 + \frac{i}{2}\Delta t\hat{A}\right)^{-1}\left(1 - \frac{i}{2}\Delta t\hat{A}\right) + O(\Delta t^3), \tag{20}$$

which ensures the desired accuracy of the numerical algorithm (19). Thus, after the discretization of r (or ρ_R) with the help of finite differences the matrix $\hat{A}$ possesses a band structure, and we arrive at the following boundary-value problem:

$$\left(1 + \frac{i}{2}\Delta t\hat{A}\right)\psi\left(t_n + \frac{\Delta t}{4}\right) = \left(1 - \frac{i}{2}\Delta t\hat{A}\right)\psi(t_n),$$

which can be solved rapidly due to the band structure of the matrix $\hat{A}$. This computational scheme is unconditionally stable [20], preserves unitarity, and is very efficient, i.e., the computational time is proportional to the total number of grid points. The efficiency of the computational procedure is based on the fast transformation with the help of the unitary matrix $S_{j\nu} = \lambda_j^{1/2} Y_{j\nu}$ between the two relevant representations: the two-dimensional DVR (14) and the Y_ν representation (16).

IV. MODELING FINITE-RANGE ATOMIC INTERACTIONS

In this section we introduce our finite-range two-body interaction potential $V(r)$ and analyze its scattering properties in 3D free space. Subsequently, in the next section, we will use this potential in order to explore interatomic collisions in harmonic confinement. Naturally, the main interest focuses on regions of resonant or near-resonant scattering. A first approach to analyzing the CIR beyond the s-wave zero-range

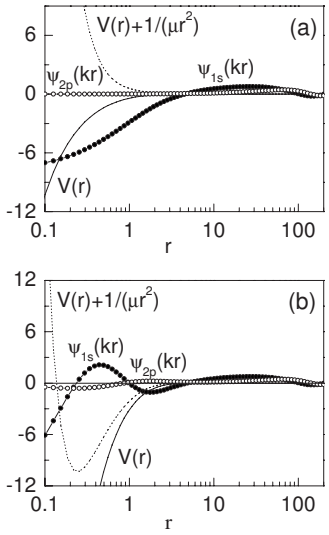

FIG. 1. (a) s- and p-wave scattering wave functions $\psi_{1s}(kr)$ and $\psi_{2p}(kr)$ (normalized to unit amplitude $\rightarrow \sin(kr-\pi/2l+\delta_l)/(kr)$ for $r\rightarrow\infty$), together with the corresponding interatomic potentials $V(r)+l(l+1)/(2\mu r^2)$. Calculations are performed for $V_0=-1.136$, $\mu=1$, leading to a single bound state in the s-wave potential (the scattering function possesses a single node as a function of r in the region where the potential acts) and a completely repulsive interaction for the p wave (no nodes with respect to r in the same region). The collision energy is $E=5\times10^{-4}$. Cases shown correspond to the following s- and p-wave scattering parameters: $a_s(E)=+4.543$ and $V_p(E)=-1.677$. (b) The same as in (a) but now for a deeper interatomic potential $V_0=-8.45$, leading to three bound states in the s-wave potential (see the three nodes with respect to r in the region where the potential acts) and one bound state in the p-wave potential (a single node with respect to r in the same region). Collision energy is $E=5\times10^{-4}$. The resulting s- and p-wave scattering parameters are $a_s(E)=+4.799$ and $V_p(E)=-48.20$. All quantities are given in units according to Eqs. (6) and (7).

pseudopotential approach was undertaken in Ref. [8] for the case $\omega_1=\omega_2$. It was shown that the CIR occurs not only for a zero-range s-wave pseudopotential but also for finite-range models of the interatomic interactions $V(r)$: the spherical square well and the "C_6-C_{12} potential" $V(r)=-C_6/r^6+C_{12}/r^{12}$. Moreover, it has been shown that the scattering amplitude is rather insensitive to the details of the interatomic interaction potential in the region of the CIR. This is why we choose a simple form for the short-range potential which can be easily tuned in order to explore the variety of possible effects occurring in a confinement due to changes of the spectral structure of the potential. This should not obscure the fact that investigations employing real molecular interaction potentials are very desirable. Here we focus on the interatomic interaction modeled by the screened Coulomb potential

$$V(r) = V_0 \frac{r_0}{r} e^{-r/r_0}, \tag{21}$$

which has in the past been extensively applied for investigations of the quantum dynamics of various few-body problems (see, e.g., Refs. [21,22]). If the length scale r_0 is fixed in (21), the potential depends on a single parameter V_0. It has two remarkable advantages compared to the zero-range s-wave pseudopotential: first, by varying V_0 one can vary the number of bound states, in particular those of s-wave character, and, second, we can create new bound and resonant states of higher partial-wave character. It is evident that varying the length scale r_0 instead of V_0 yields similar effects. Beyond these important features, the smoothness of the screened Coulomb potential allows for a numerically stable and efficient integration of the corresponding time-dependent Schrödinger equation. In conclusion, the model potential (21) represents a generalization of the pure s-wave pseudopotential approach and exhibits a much richer spectral structure. This will, as we shall see below, permit us to explore new regimes and effects of confined scattering processes.

TABLE I. The dependence of the s- and p-wave scattering parameters $a_s(E)$ and $V_p(E)$ on the collision energy E, calculated for the free-space scattering potential $V(r)+l(l+1)/2\mu r^2$. Also provided are the values of the parameter $a_\perp/a_s$ adopted for the chosen coupling constant V_0 in the single-mode regime of the harmonic confining potential with frequency $\omega=0.02$. All quantities are given in units according to Eqs. (6) and (7).

V_0	$a_\perp/a_s$	E	$a_s(E)$	$V_p(E)$
−1.136	1.56	0.0005	4.543	−1.677
		0.001	4.526	−1.669
		0.002	4.492	−1.652
		0.004	4.426	−1.666
−8.45	1.47	0.0005	4.799	−48.20
		0.001	4.790	−49.05
		0.002	4.773	−50.83
		0.004	4.740	−54.81

Before starting the investigation of the scattering process in the presence of confinement, it is instructive to analyze the corresponding free scattering behavior of the potential (21). We assume $r_0=1$ and vary the "coupling constant" V_0. Let us focus on two cases: (a) there is one s-wave bound state for the potential (21) and a repulsive p-wave potential obtained by choosing the coupling constant close to the value $V_0=-1.136$; (b) there are three bound states of s-wave character and one p-wave bound state for values of V_0 close to −8.45. These two cases are illustrated in Fig. 1, where the s- and p-wave scattering functions are shown together with the corresponding interatomic potentials $V(r)+l(l+1)/2\mu r^2$. The dependence of the s-wave and p-wave scattering parameters

$$a_s(E) = -\frac{\tan\delta_s(E)}{k} \rightarrow a_s, \quad V_p(E) = -\frac{\tan\delta_p(E)}{k^3} \rightarrow V_p$$

on the collision energy E for $E\rightarrow0$ ($k=\sqrt{2\mu E}\rightarrow0$) is provided in Table I. The calculation of $a_s(E)$ and $V_p(E)$ was performed within a sixth-order finite-difference approach [17] on a quasiuniform grid [16]. Due to the spherical symmetry of the interaction (21), the angular motion separates for the free 3D scattering problem, resulting in numerical integration of the radial Schrödinger equation only.

The data presented in Fig. 1 and Table I demonstrate that by decreasing the coupling constant V_0 one can model a near-threshold resonant or bound state of p-wave character, and the corresponding scattering volume V_p takes on very large values, specifically, $|V_p| \to 47.4$ for $V_0 = -8.45$. The p-wave scattering length is then $a_p = V_p^{1/3} = -3.6$, which is in absolute value comparable with the s-wave scattering length $a_s = 4.8$. Thus, by varying the coupling strength V_0 from $V_0 = -1.136$ to -8.45, we can easily transform the standard problem of pure s-wave scattering to the situation of simultaneous large s- and p-wave scattering lengths, i.e., both partial waves are nearly resonant with respect to their free-space scattering. In the following, we will explore, among other topics, the impact of this combined resonant behavior on the scattering properties under confinement, addressing both the separable $\omega_1 = \omega_2$ and nonseparable $\omega_1 \neq \omega_2$ cases.

V. RESULTS AND DISCUSSION

We will first investigate collisions of two identical particles in the transversal ground state, i.e., the single-mode regime, of a harmonic cylindrical waveguide with $\omega_1 = \omega_2$. The latter allows for a separation of the c.m. and relative motions, and the corresponding partial waves are exclusively either even or odd. Subsequently, we will explore the more general case of heteronuclear collisions in the waveguide involving two distinguishable atoms. In this case the c.m. and relative motions are coupled via the term $\mu(\omega_1^2 - \omega_2^2)\rho_R \rho \cos(\phi)$, mixing even and odd partial waves if $\omega_1 \neq \omega_2$. The case of a single mode and scattering of a single species is naturally divided into two subtopics, which were addressed already in Refs. [3,8–10]. First, this is the symmetric case $f_u = 0$ describing collisions of two bosons and, second, it is the antisymmetric case $f_g = 0$ representing collisions of two fermions. The latter is again divided into two subsections. First, this is the case where both distinguishable particles are in the same harmonic trap with equal trap frequencies $\omega = \omega_1 = \omega_2$, where, however, the scattering amplitude $f \to f_g \pm f_u$ should not be (anti)symmetrized as for identical particles. The second case is the most general one where the colliding distinguishable particles experience different trap frequencies $\omega_1 \neq \omega_2$, leading to the nonseparability of the c.m. and relative motions and consequently to strong partial-wave mixing.

A. Single atomic species in a harmonic waveguide

1. Bosonic scattering under harmonic confinement

This case has already been explored in the s-wave zero-range pseudopotential approach both analytically and numerically in Refs. [3,8,9,11,12]. We will use the corresponding results for comparison and to analyze certain computational aspects of our approach. In the case of collisions of identical bosons under a harmonic confinement, the frequency of the confinement is the same for all atoms, $\omega_1 = \omega_2 = \omega$. Consequently, the term proportional to $\rho\rho_R \cos\phi$ does not occur in our Hamiltonian $H^{(0)}$ [see Eq. (7)], the c.m. and relative motions separate, and our scattering problem reduces to a two-dimensional one involving the degrees of freedom (r, θ). To fix the conditions analogous to the symmetric case ($f_u = 0$) of pure s-wave scattering approximated in the s-wave pseudopotential approach, we choose the atom-atom interaction operator in the form $\hat{V}(r) = V(r)\delta_{l,0}$, where the potential function $V(r)$ has been defined in Eq. (21). This interaction operator scatters only s waves, leading to $f_g(k) = f^+(k)$, and one can define the quasi-1D coupling constant g_{1D} in Eq. (12) by calculating the forward scattering amplitude $f^+(k)$ given in Eq. (11). Following Refs. [3,8,9,11,12], we analyze the dependence of the scattering amplitude on the parameter $a_\perp / a_s$ near the resonant value $a_\perp / a_s = 1.4603\ldots$ found in [3] in the s-wave zero-range pseudopotential approach. Here, $a_\perp = \sqrt{2/\mu(\omega_1 + \omega_2)} = \sqrt{1/\mu\omega}$ is the confinement (oscillator) width and a_s is the s-wave scattering length describing the atom-atom collision in 3D free space in the zero-energy limit. We choose the oscillator frequency of the confining potential in the regime $0.005 \leq E_\perp = \omega \leq 0.02$ and comparatively low longitudinal relative energies according to $0.002 \leq \varepsilon \leq 0.004$, which are well below the energy of the first transversally excited channel. We are therefore studying collision processes in the single-mode regime $\omega < E = E_\perp + \varepsilon < 3\omega$. The chosen interval of collision energies is in the region where the approach employing just the scattering length as a single parameter already provides a qualitatively correct description of the scattering process (see Table I). The longitudinal width of the initial wave packet in Eq. (8) is chosen sufficiently broad according to $a_z = 1/\sqrt{\mu\omega_z} \approx 30-40$ to satisfy the demand of sufficient monochromaticity of the wave packet along the z direction (ω_z is introduced here, although there is no confining potential in the z direction, in order to account for the energy uncertainty of the z motion of the wave packet). Consequently, the spreading is

$$D_z(t) = \langle \psi(t) | (z - \bar{z})^2 | \psi(t) \rangle \to a_z^2/2[1 + t^2/(\mu^2 a_z^4)]_{t=0} \approx 5 \times 10^2 \tag{22}$$

and the small dispersion of the longitudinal momentum reads $D_k = \langle \psi(t) | (k - \bar{k})^2 | \psi(t) \rangle \to 1/(2a_z^2) \approx 5 \times 10^{-4}$. The variation in time of the calculated dispersion $D_z(t)$ together with an expected estimate of it are presented in Table II and discussed below [see the second paragraph after Eq. (23)]. The initial localization of the wave packet is on the negative semi-half-axis $z < 0$, out of the range of the interatomic potential, i.e., out of the scattering region. We choose $z_0 = -60$ and obtain for $\langle \psi(t=0) | \psi(t=0) \rangle$ (integrating over the subspace $z < 0$) a deviation from 1 which is less than 0.5%, corresponding to the typical accuracy of our computations.

To model the conditions $a_\perp / a_s \sim 1.46$ of the s-wave ultracold atom-atom collisions in the harmonic trap near the CIR, explored in Refs. [3,8], we fixed the oscillator width according to $a_\perp = 1/\sqrt{\mu\omega} \approx 7$ ($\omega \approx 0.02$), and the atom-atom s-wave scattering length in free space a_s was changed by varying the interatomic coupling constant $-1.3 \leq V_0 \leq -0.85$ in the vicinity of the value $V_0 = -1.136$, which provides an s-wave scattering length a_s such that $a_\perp / a_s \approx 1.46$. We have calculated the wave packet $\psi(r, \theta, t)$ time evolution from $t = 0$ up to $t \approx (10-15)t_0$ (depending on the collision energy) in units of

TABLE II. Calculated values of the mean wave-packet energy $\bar{E}(t)$ (23) and the wave-packet dispersions $D_z(t)$ and $D_\rho(t)$ in z and ρ directions together with the corresponding theoretical estimates for these values: $\bar{E}^{th}=\omega+\omega_z+\varepsilon=0.02+0.001+0.004=0.025$. D_z^{th} was evaluated from the free-space limit (22) and D_ρ^{th} from the corresponding expression for the two-dimensional oscillator potential $D_\rho^{th}=a_\perp^2(1-\pi/4)=1/\omega(1-\pi/4)=10.7\ldots$. Parameter values are $V_0=-1$, $\omega=0.02$, $N_\theta=60$, $N_r=200$, and $\varepsilon=0.004$, and consequently $a_\perp/a_s=0.907$. All quantities are given in units according to Eqs. (6) and (7).

t/t_0	$\bar{E}(t)$	$\bar{E}^{th}$	$D_z(t)$	$D_z^{th}(t)$	$D_\rho(t)$
0.1	0.02440	0.0250	500	500	10.7
1.0	0.02440	0.0250	447	534	10.6
2.0	0.02440	0.0250	299	637	11.2
3.0	0.02439	0.0250	365	808	10.4
4.0	0.02439	0.0250	856	1050	11.2
5.0	0.02439	0.0250	1580	1360	10.0
6.0	0.02438	0.0250	2490	1730	9.90

$t_0=2\pi/(\omega+\varepsilon)$. Within this time period, the wave packet splits under the action of the interatomic potential but does not reach the boundaries of the grid, which have been chosen at $z=\pm 200$. We compute the mean value of the interatomic energy via

$$\bar{E}(t)=\left\langle \psi(t)\left| i\frac{\partial}{\partial t}\psi(t)\right.\right\rangle, \tag{23}$$

the dispersions $D_z(t)$ and $D_\rho(t)$, and the scattering amplitude f^+ [see Eq. (12)]. The calculations were done on a radial grid $\{r_j\}$ with the number of grid points N_r varying in the interval $80\leq N_r\leq 200$ to check the convergence of the computations. For the same reason the number of angular grid points N_θ was varied according to $20\leq N_\theta\leq 60$. $\bar{E}(t)$, $D_z(t)$, $D_\rho(t)$, $f^+(t)$, and the transmission coefficients $T(t)=|1+f^+(t)|^2$ are presented for a few values of $a_\perp/a_s$ in Table II and in Fig. 2. Figure 2 also shows the transmission coefficient $\tilde{T}(t)$, calculated by the integration of the probability density $\tilde{T}(t)=\int_{r_0}^{\infty}\int_0^{\pi/2}|\psi(r,\theta,t)|^2 dr\sin\theta\, d\theta$ over the part of the semi-half-space $z>0$ that is out of the action of the interatomic potential $z>z_0=r_0\cos\theta\approx 1$. Also provided in Fig. 2 is the effective 1D coupling constant $g_{1D}(t)$ calculated via Eq. (12).

Table II shows for a certain set of time instants the evolution of the mean value of the wave-packet energy $\bar{E}(t)$, which is close to the sum of the transversal and longitudinal energies, $\bar{E}^{th}=\omega+\omega_z+\varepsilon$. The time evolution of the longitudinal dispersion $D_z(t)$ of the wave packet follows the expression (22) (valid for the wave-packet spreading in free space) only for very short times $t\ll t_0$, where it does not overlap with the scattering region. The evolution of the transverse dispersion $D_\rho(t)$ qualitatively reproduces the corresponding value for the two-dimensional oscillator for long propagation times.

Figure 2 demonstrates the convergence of the scattering amplitude $f^+(t)$ for $t\to\infty$ according to Eq. (11). We observe that the amplitude $f^+(t)$ reaches its asymptotic value $f^+(t\to\infty)$ already for times $t\gtrsim(3-4)t_0$ in the complete regime of varying interaction strength, leading to $0.5a_\perp\lesssim a_s\lesssim 4a_\perp$. Figure 2 also shows the effective quasi-1D coupling constant $g_{1D}(t)$ [see Eq. (12)] and the transmission coefficient $T(t)=|1+f^+(t)|^2$ as a function of time. Obviously, the most difficult task is to accurately evaluate the value of the quasi-1D coupling constant $g_{1D}(a_\perp/a_s)$ in the region $a_\perp/a_s\sim 1.46$ close to the CIR because of the smallness of $\mathrm{Im}[f^+(a_\perp/a_s)]$. The relative accuracy of the computed value of g_{1D} decreases near the CIR. However, the position of the CIR itself is provided quite accurately by calculating the position of the zero of the function $\mathrm{Im}[f^+(a_\perp/a_s)]$.

Figure 2 demonstrates that the transmission coefficients $T(t)$ and $\tilde{T}(t)$, calculated in the two different ways described above, approach very similar values in the asymptotic region. This holds even in the region $a_\perp/a_s\approx 1.46\ldots$ of the CIR. Principally, the computational scheme for the coefficient $T(t)$ is more accurate since the definition of $\tilde{T}$ contains the uncertainty related to a not well-defined boundary of the scattering region. The convergence of the calculated effective quasi-1D coupling $g_{1D}(t)$ to the asymptotic value $g_{1D}(\infty)$ is considerably slower than the convergence of the transmission coefficients $T(t)$ and $\tilde{T}(t)$. However, the results provided in Fig. 2 demonstrate that by integrating up to $t\sim(7-8)t_0$ one can obtain also the coupling g_{1D} in the region near the CIR. The oscillations in time of the calculated scattering parameters, especially amplified for the case of the $g_{1D}(t)$ function near the resonant region $a_\perp/a_s\approx 1.46$, represent the Fourier component related to the weakly bound molecular state $2E_B\sim -1/a_s^2$. The value of the binding energy E_B defines the period of the oscillations, $T_B\sim 2\pi/E_B\sim 4\pi a_s^2$, in $g_{1D}(t)$ and decreases considerably, as is qualitatively reproduced by the above simple estimate, as the scattering length a_s varies from $a_\perp/0.248$ to $a_\perp/2.08$.

For comparison with the literature [3,8], we have calculated the effective quasi-1D coupling constant $g_{1D}(a_\perp/a_s)$ and the transmission coefficient $T(a_\perp/a_s)$ as a function of the ratio $a_\perp/a_s$ in the region $1\leq a_\perp/a_s\leq 2$ near the CIR. The corresponding results are presented together with $f^+(a_\perp/a_s)$ in Fig. 3. The CIR, originally predicted for a zero-range s-wave pseudopotential [3] at $a_\perp/a_s=1.46$, is clearly observed in our wave-packet dynamical simulation. However, its position is shifted to slightly larger values: At $\varepsilon=0.004$ we obtain $a_\perp/a_s=1.48$ for the CIR position. On decreasing the longitudinal collision energy ε to 0.002 and then 0.001, it converges to $a_\perp/a_s=1.47$. A similar shift of the position of the CIR, calculated for a spherical well potential as well as for a Lennard-Jones C_6-C_{12} potential, was also found in Ref. [8]. The corresponding transmission coefficient $T(a_\perp/a_s)$ exhibits a well-pronounced minimum (total reflection of the atoms) at the position of the CIR, where $f^+\to -1$ and $T=|1+f^+|^2\to 0$ hold when approaching the resonance. The data presented in Fig. 3 for the scattering amplitudes $f^+(a_\perp/a_s)$ were evaluated near the point of the CIR by averaging over time,

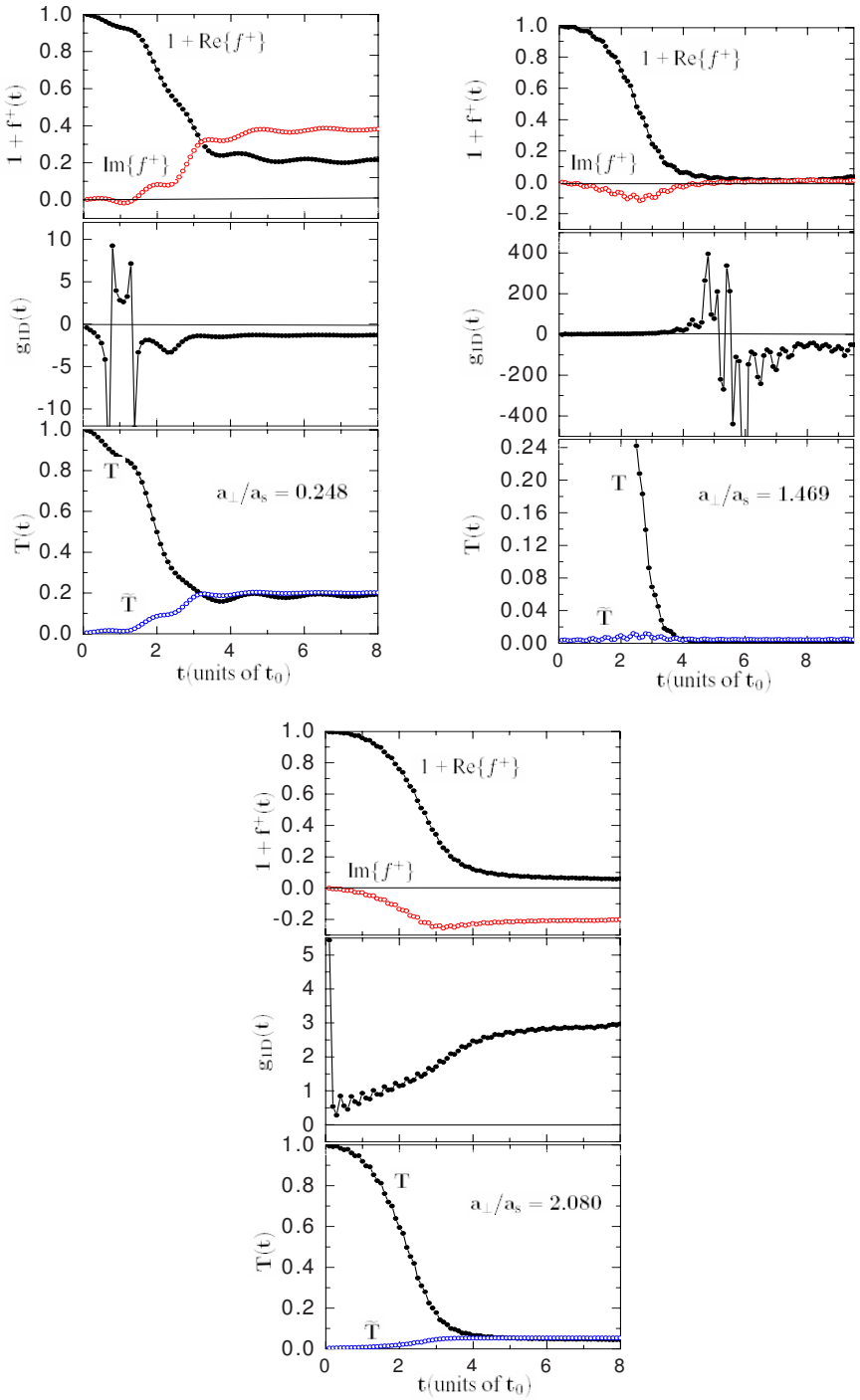

FIG. 2. (Color online) Time evolution of the scattering amplitude $f^{+}(t)=f_g(t)$, the effective quasi-1D coupling constant $g_{1D}(t)$, and the transmission coefficients $T(t)$ and $\tilde{T}(t)$ for different values of $a_\perp/a_s$: far below the CIR $a_\perp/a_s=0.248$, near the CIR $a_\perp/a_s=1.469$, and far above the CIR $a_\perp/a_s=2.080$. The calculations are performed for scattering of identical bosons in a harmonic trap with $\omega_1=\omega_2=0.02$, for the longitudinal collision energy $\varepsilon=0.004$. V_0 is varied within the region $-1.3\leq V_0\leq -0.85$. Time t is given in units of $t_0=2\pi/(\omega+\varepsilon)$; the effective quasi-1D coupling constant g_{1D} in units of $1/(\mu a_\perp)$.

$$\langle f^{+}(a_\perp/a_s)\rangle = \frac{1}{t_{max}-t_{asym}}\int_{t_{asym}}^{t_{max}} f^{+}(a_\perp/a_s,t)dt$$

in the asymptotic region $t\gtrsim t_{asym}=(7-8)t_0$. The functions $g_{1D}(a_\perp/a_s)$ and $T(a_\perp/a_s)$ were then calculated employing the mean values of $\mathrm{Re}[\langle f^{+}(a_\perp/a_s)\rangle]$ and $\mathrm{Im}[\langle f^{+}(a_\perp/a_s)\rangle]$. The calculated scattering amplitude $f^{+}(a_\perp/a_s)$ is excellently fitted by the expression $f_g(\delta_g)=-(1+i\cot\delta_g)^{-1}$ (see [11,13,14]) in the complete region $1\leq a_\perp/a_s\leq 2$, employing the single fitting parameter δ_g, which approaches $\delta_g(\varepsilon=0.004)=\pi/2$ at the point $a_\perp/a_s=1.48$ of the CIR.

After this first application of our wave-packet dynamical approach to the well-known case of the bosonic CIR, we extend our investigation in the following sections to the case of scattering of two identical fermions ($f_g=0$) under a harmonic confinement as well as to the effects of partial-wave mixing due to the nonseparability of the c.m. and relative motions in a harmonic confinement for distinguishable particles.

2. Fermionic scattering under harmonic confinement

In this section we analyze pure p-wave scattering of fermions ($\omega_1=\omega_2$) under the action of the potential $\hat{V}(r)$

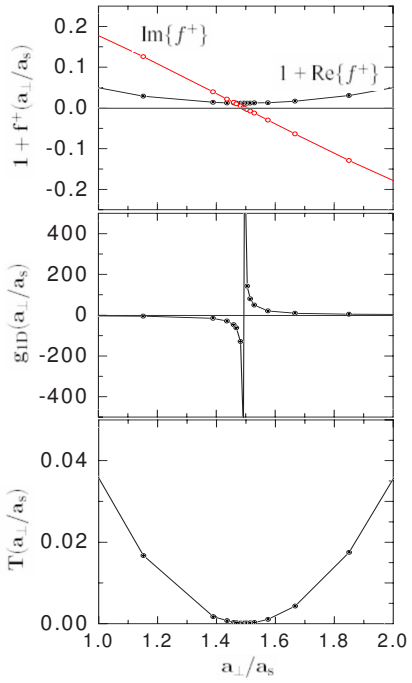

FIG. 3. (Color online) Scattering amplitude $f^+(a_\perp/a_s)=f_g(a_\perp/a_s)$, effective quasi-1D coupling constant $g_{1D}(a_\perp/a_s)$, and transmission coefficient $T(a_\perp/a_s)$ calculated for the symmetric case $f_u=0$ of bosonic scattering for $V(r)\delta_{l0}$ in a harmonic confinement $\omega_1=\omega_2=0.02$, for $\varepsilon=0.004$. The coupling constant V_0 is varied in the region $-1.3\leq V_0\leq -0.85$. The effective quasi-1D coupling constant g_{1D} is provided in units of $1/(\mu a_\perp)$.

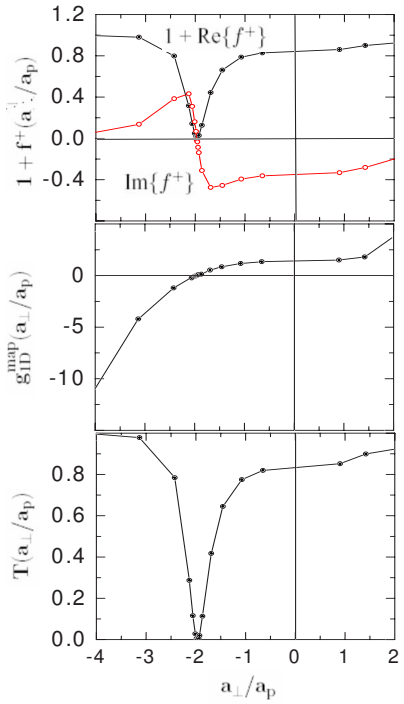

FIG. 4. (Color online) Scattering amplitude $f^+(a_\perp/a_p)=f_u(a_\perp/a_p)$, mapped coupling constant $g_{1D}^{map}(a_\perp/a_p)$, and transmission coefficient $T(a_\perp/a_p)$ for the antisymmetric case $f_g=0$ of fermionic scattering defined by the interatomic operator $V(r)\delta_{l1}$ in a harmonic confinement $\omega_1=\omega_2=0.02$ for $\varepsilon=0.004$. The coupling constant V_0 is varied in the region $-9.5\leq V_0\leq -7.5$. The mapped coupling constant g_{1D}^{map} is provided in units of $1/(\mu a_\perp k^2)$.

$=V(r)\delta_{l,1}$ in a harmonic trap analogous to the one discussed in the previous section. By choosing the coupling constant V_0 close to the value $V_0=-8.45$ indicating the appearance of a bound molecular state in the p-wave [see Fig. 1(b)] we model a resonant scattering of spin-polarized fermions ($f_g=0$) in a harmonic confinement [10,23]. In Fig. 4 we present the calculated p-wave scattering amplitude $f^+(a_\perp/a_p)$ in a region $-4\leq a_\perp/a_p\leq 2$ including the position of the resonance. Here also the calculated "mapped coupling constant" $g_{1D}^{map}=\lim_{k\to 0}\mathrm{Im}[f^+(k)]/(\mathrm{Re}[f^+(k)]\mu k)$ [10] and the transmission coefficient T are illustrated. The position of the zero of the mapped coupling constant for the fixed value $\varepsilon=0.004$ is at the point $a_\perp/a_p=-1.97$, close to the value $a_\perp/a_p=-2$ obtained in Refs. [11,14]. Close to the position of the p-wave resonance, the scattering amplitude f^+ behaves as $f^+\to -1$ and, as a consequence, $T=|1+f^+|^2\to 0$, i.e., we obtain strongly interacting and impenetrable fermions (see the corresponding panel of Fig. 4 demonstrating the transmission behavior). The latter can be mapped on a system of free bosons [10], as can be seen also from our wave-packet dynamical simulations, showing in Fig. 4 that g_{1D}^{map} possesses a zero at resonance.

As in the previous section devoted to pure s-wave scattering ($f_u=0$) in a harmonic confinement, we also find here an excellent fit of the calculated scattering amplitude $f^+(a_\perp/a_p)$ for the case $f_g=0$ of pure p-wave scattering in the complete region $-4\leq a_\perp/a_p\leq 2$ by the expression $f_u(\delta_u)=-(1+i\cot\delta_u)^{-1}$ (see [11,13,14]), with one fitting parameter δ_u approaching $\delta_u(\varepsilon=0.004)=\pi/2$ at the point $a_\perp/a_p=-1.97$ of the resonance.

B. Different atomic species in a harmonic waveguide

1. Scattering of distinguishable particles under harmonic confinement $\omega_1=\omega_2$

In the case of two distinguishable particles colliding in the same harmonic trap with $\omega_1=\omega_2$, the c.m. motion separates but now s and p states both provide contributions to the scattering amplitude $f^+=f_g+f_u$. Such a case can be realized in a magnetic trap if the distinguishable atoms possess the same value for the product of their g factor and the projection of their total magnetic moment onto the magnetic field axis. The computational scheme we follow here is analogous to the one considered in the previous sections, with the only difference that the interaction potential now acts on all possible partial waves and is defined by Eq. (21). The results of the calculations of the scattering amplitudes $f^+(a_\perp/a_s)$ and $f^+(a_\perp/a_p)$ are illustrated in Fig. 5 for the regions $1\leq a_\perp/a_s\leq 2$ and $-4\leq a_\perp/a_p\leq 2$ analyzed before for the scattering of bosons. In the first region $1\leq a_\perp/a_s\leq 2$ ($V_0\sim -1.14$), with one s-wave bound state and no bound states of higher partial waves [see Fig. 1], the main contribution to the scattering amplitude f^+ is provided by the s-wave partial amplitude f_g [see Fig. 5(a)]. However, the fitting formula with the param-

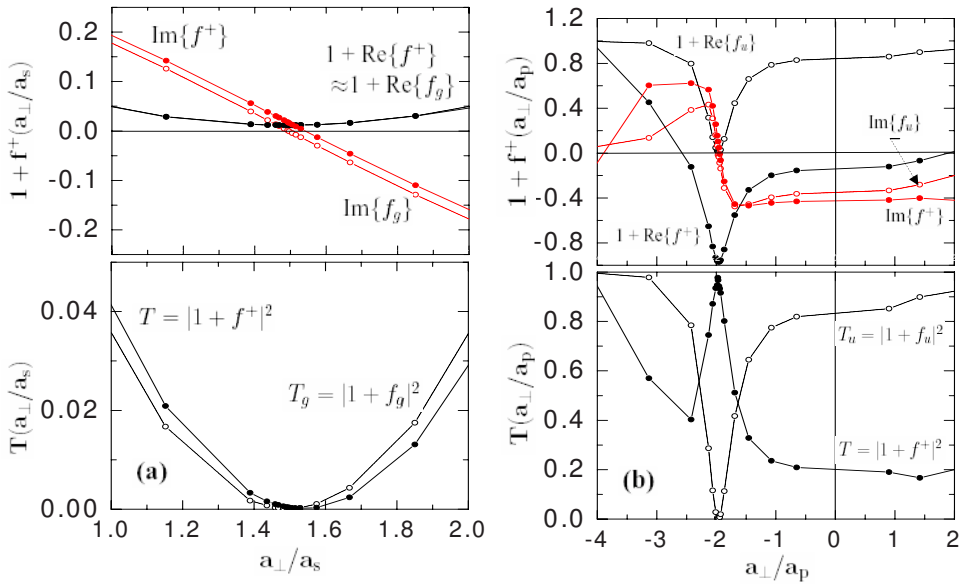

FIG. 5. (Color online) (a) Scattering amplitudes $f^+(a_\perp/a_s)$ and $f_g(a_\perp/a_s)$ and corresponding transmission coefficients $T(a_\perp/a_s)=|1+f^+(a_\perp/a_s)|^2$ and $T_g(a_\perp/a_s)=|1+f_g(a_\perp/a_s)|^2$ for scattering of distinguishable and identical (bosonic) atoms in a harmonic confinement $\omega_1=\omega_2=0.02$ for $\varepsilon=0.004$. In both cases the interatomic interaction is described by the same potential function (21); however, the interaction operator is acting on both even and odd waves for scattering of distinguishable atoms and exclusively on the s waves for scattering of identical bosons. The coupling constant V_0 is varied in the region $-1.3\leq V_0\leq -0.85$. (b) Scattering amplitudes $f^+(a_\perp/a_p)$ and $f_u(a_\perp/a_p)$ and corresponding transmission coefficients $T(a_\perp/a_p)=|1+f^+(a_\perp/a_p)|^2$ and $T_u(a_\perp/a_s)=|1+f_u(a_\perp/a_p)|^2$ for scattering of distinguishable and fermionic atoms in harmonic confinement $\omega_1=\omega_2=0.02$, at $\varepsilon=0.004$. In both cases the interatomic interaction is described by the same potential function (21); however, the interaction operator is acting on both even and odd waves for the scattering of distinguishable particles and exclusively on the p waves for scattering of identical fermions. The coupling constant V_0 varies within the region $-9.5\leq V_0\leq -7.5$.

eter δ_g used previously must be replaced by the two-parameter function [11]

$$f^+ = -\frac{1}{1+i\cot\delta_g}-\frac{1}{1+i\cot\delta_u}. \tag{24}$$

This leads to a separation of the positions of the zero of the function $\mathrm{Im}[f^+(a_\perp/a_s)]$ and the minimum of the function $\mathrm{Re}[f^+(a_\perp/a_s)]$ on the axis $a_\perp/a_s$. As a result, the position of the minimum of the transmission coefficient $T(a_\perp/a_s)$ is also shifted when compared to its position in the case of pure s-wave scattering, i.e., to $|1+f_g(a_\perp/a_s)|^2$.

Our second focus is the region $-4\leq a_\perp/a_p\leq 2$, corresponding to values $V_0\sim -8.45$, where we encounter s- and p-wave contributions for the scattering in 3D free space [see Fig. 1(b)] that are of the same order of magnitude [13,14]. In this case, we have a combined resonant 3D scattering process in free space where both partial waves significantly contribute to the total scattering cross section

$$\sigma=\frac{4\pi}{k^2}\sum_l (2l+1)\sin^2\delta_l.$$

Surprisingly, it turns out that the corresponding scattering in the presence of harmonic confinement can be completely suppressed; this happens because of destructive interference of the s and p waves in the effective 1D quantum scattering process of the strongly interacting particles. This is the so-called dual CIR predicted first in [13]. This effect is illustrated in Fig. 5(b) by showing the quantity $1+f^+(a_\perp/a_p)$ together with the transmission coefficient $T(a_\perp/a_p)$. The destructive interference of the s- and p-wave scattering processes under the action of the confinement transforms the total reflection of the pure p-wave scattering $T=|1+f_u|^2\to|1-1|^2\to 0$ at the point of resonance $a_\perp/a_p=-1.98$ (see Fig. 4) to the total transmission $T=|1+f_g+f_u|^2\to|1-1-1|^2\to 1$ for the combined p- and s-wave scattering in the trap. In conclusion, we obtain complete transmission through destructive interference of even and odd partial waves in the guide.

In Fig. 6 we demonstrate how the 3D scattering cross section $\sigma(V_0)$ belonging to the potential (21) in free space is transformed under the action of the harmonic confinement into the reflection coefficient $R(V_0)=1-T(V_0)$ of the quasi-1D scattering. In free-space scattering we encounter two resonant regions of the coupling constant of the interaction potential (21) near the points $V_0=-0.78$ and -8.85 [see Fig. 6(a)], respectively. The first resonance at $V_0=-0.78$ in Fig. 6(a) is a pure s-wave scattering resonance in free space [Fig. 6(b)], which transforms into complete reflection $R\approx 1$ in the case of quasi-1D scattering in a harmonic confinement corresponding to $a_\perp/a_s=1.48$; see Fig. 6(c). The corresponding 3D scattering cross section exhibits a pronounced maximum near the position $V_0=-1.12$ of complete reflection. The second resonance is a p-wave shape resonance of free-space scattering which occurs at $V_0=-8.85$ [see Fig. 6(a)]. At $V_0=-8.45$ both s- and p-wave scattering are strong, and the corresponding scattering lengths are simultaneously large. As a result we obtain complete transmission in a harmonic waveguide or, as can be seen from Fig. 6(c), a zero of the

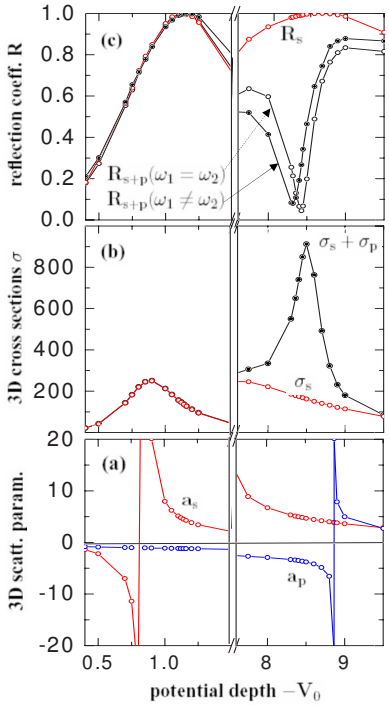

FIG. 6. (Color online) (a) s- and p-wave scattering lengths $a_s(V_0)$ and $a_p(V_0)$; (b) corresponding s-wave and total 3D scattering cross sections $\sigma_s(V_0)$ and $\sigma(V_0)=\sigma_s(V_0)+\sigma_p(V_0)$ in free space; and (c) s-wave and total reflection coefficients $R_s(V_0)$ and $R(V_0)$ describing the scattering for the separable case $\omega_1=\omega_2=0.02$ and the nonseparable case $\omega_1/1.35=\omega_2=0.02$ of harmonic confinement. All quantities are given in units according to Eqs. (6) and (7); $\varepsilon=0.004$.

reflection coefficient at $V_0=-8.45$. The corresponding total 3D cross section [see Fig. 6(b)] exhibits a maximum for this value of V_0.

Let us discuss the aforementioned results in the framework of the time evolution of the wave packet. Figure 7(a) demonstrates the time evolution of the wave packet in the waveguide for the case of nonresonant scattering in free space ($V_0=-0.6$ in Fig. 6). The wave packet is split by the action of the interatomic potential into reflected and transmitted parts moving in opposite directions after the collision. The peak of the probability function $|\psi(z,\rho=0,t)/r|^2$ remaining at the origin $z=0$ after the collision indicates a resonant collisional behavior reminiscent of the considerations provided in Ref. [8]. At $V_0=-1.12$, we are close to the s-wave CIR and observe complete reflection of the wave packet for the scattering process in the wave guide; see Fig. 7(b). Here the resonant behavior mentioned above is even more pronounced. In the case of the dual CIR [13,14], at $V_0=-8.45$ complete transmission is obtained [see Fig. 7(c)]. We therefore encounter an effective transparency in the atomic scattering process in the case of the dual CIR. The resonant behavior is quite strong here too.

2. *Scattering of distinguishable particles in a waveguide* $\omega_1 \neq \omega_2$

Let us consider the most general case of a scattering process of two distinguishable particles in a harmonic confinement with different trap frequencies for the two atoms. This case, $\omega_1 \neq \omega_2$, leads to nonseparability of the c.m. motion of the colliding atoms due to the coupling term $\mu(\omega_1^2-\omega_2^2)\rho_R\rho\cos\phi=\mu(\omega_1^2-\omega_2^2)\rho_R r\sin\theta\cos\phi$ appearing in the Hamitonian $H^{(0)}$ (7). It also leads to a strong mixing of partial waves of g and u symmetry. To investigate this case, we solved the corresponding 4D time-dependent Schrödinger equation (6)–(8) for the time evolution of the wave packet $\psi(\rho_R,\rho,\theta,\phi,t)$ in the course of the collision. The numerical grid for the variable ρ_R was chosen equal to the one for the variable r. The number of grid points N_ϕ for ϕ was chosen by varying N_ϕ within the limits $5\leq N_\phi\leq 9$, applying the same criteria discussed above in the context of N_θ and the definition of the grid for the θ variable [see the paragraph after Eq. (23)].

We apply our analysis to the case of a mixture of fermionic ^{40}K and bosonic ^{87}Rb atoms with the mass ratio $m_1/m_2=40/87$. It is possible to obtain a considerable frequency detuning $\omega_1/\omega_2=1.35$ with different optical traps for the atomic species [12], which results in a substantial coupling of the c.m. and relative motions. Choosing the reduced mass $\mu=m_1m_2/(m_1+m_2)=1$, we obtain $m_2=(40+87)/40$. The trap frequency for the Rb atoms is then $\omega_2=0.02$.

We have explored the effects of the confinement-induced nonseparability of the c.m. motion and the partial-wave mixing in the harmonic trap $\omega_1=1.35\omega_2$ by calculating the deviation of the scattering amplitude $f^+(\omega_1\neq\omega_2)$ and the reflection coefficient $R(\omega_1\neq\omega_2)$ from the corresponding values at equal frequencies, defining the case of separable c.m. and relative motions ($\omega_1=\omega_2=0.02$, $\mu=1$). The corresponding results are illustrated in Fig. 6(c), where the reflection coefficient $R(\omega_1\neq\omega_2)$ is shown as a function of V_0. In the region $0.5\lesssim -V_0\lesssim 1.5$ of s-wave resonant scattering in free space, the c.m. nonseparability induced by the harmonic confinement leads to a shift of the position of the maximum of the reflection coefficient from $a_\perp/a_s=1.48$ to 1.54. This shift $\Delta_R\simeq 0.06$ differs considerably from the corresponding shift $\Delta_g\simeq 0.02$ of the position of the singular point of the quasi-1D coupling constant $g_{1D}(a_\perp/a_s)$ obtained in the s-wave zero-range pseudopotential approach and zero-energy limit in Ref. [12]. There the approximation $f_u=0$ was used explicitly. In the region $7.5\lesssim -V_0\lesssim 9.5$ of comparable resonant contributions of s and p waves in the 3D scattering cross section in free space, the effects of the c.m. nonseparability lead to a more substantial change of the reflection coefficient R. The value of the minimum of the reflection coefficient increases; see Fig. 6(c). The position of the minimum of the reflection coefficient is also shifted considerably.

The time evolution of the wave packet illustrated in Fig. 7 appears to be qualitatively similar to the corresponding one in the case of confinement-induced c.m. nonseparability. Figure 8 shows the atomic probability distributions $\int|\psi(\rho_R,r,\Omega,t)|^2/(r^2\rho)d\Omega$ before, during, and after the collision for the same three cases of V_0 shown in Fig. 7: nonresonant scattering, s-wave resonant scattering, and simultaneous s- and p-wave resonant scattering. Figure 8 demonstrates the quantum dynamics with respect to both the relative and c.m. motions.

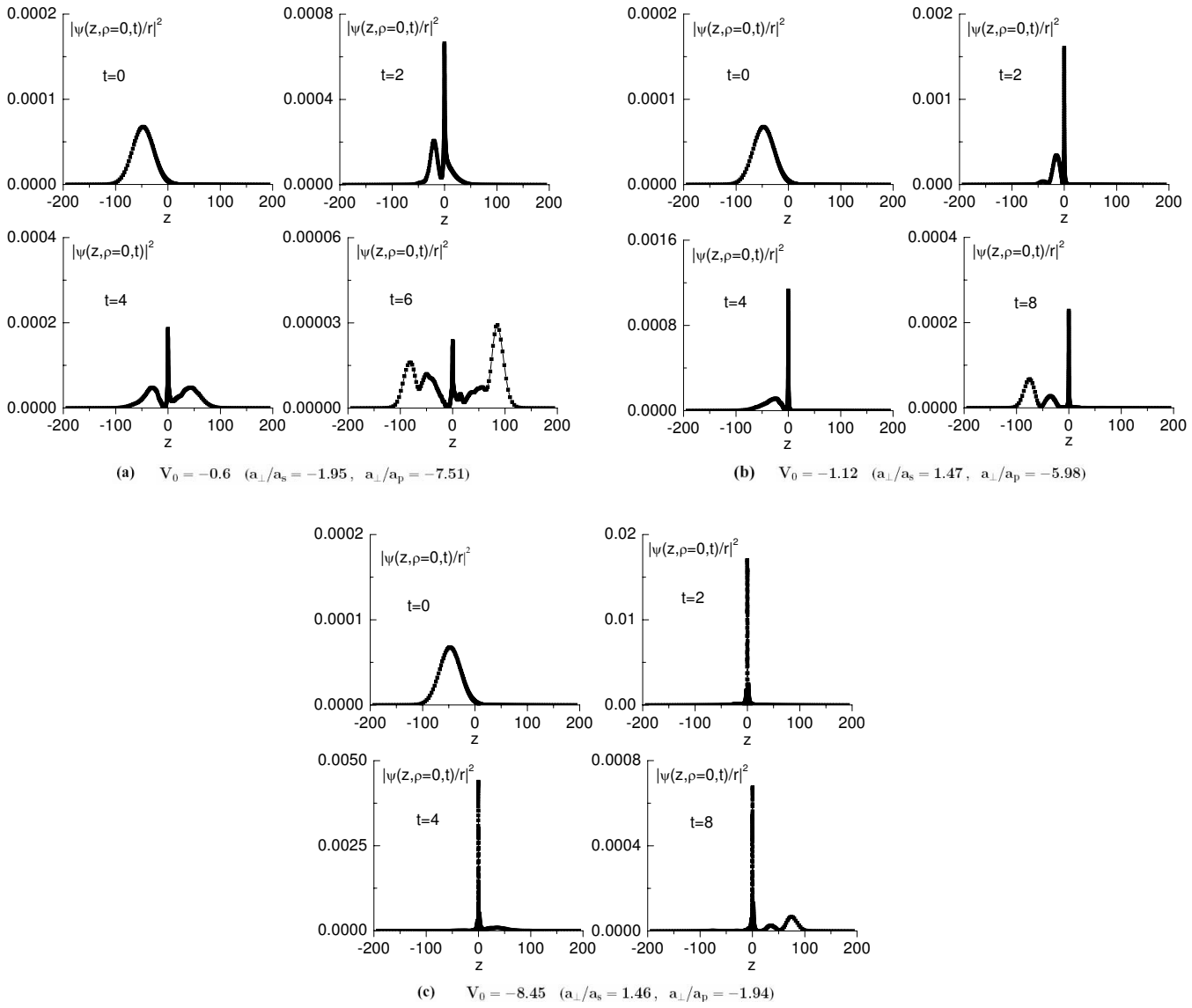

FIG. 7. Time evolution of the intersection of the probability density distribution $|\psi(z,\rho=0,t)/r|^2$ of the wave packet in the harmonic trap $\omega_1=\omega_2=0.02$ for two distinguishable particles for three cases: (a) nonresonant scattering in free space for $V_0=-0.6$, (b) s-wave resonant scattering in free space for $V_0=-1.12$ (creating a CIR in a harmonic trap), (c) simultaneous s- and p-wave resonances in free space at $V_0=-8.45$ (creating a dual CIR in a harmonic trap). Time t is given in units of $t_0=2\pi/(\omega+\varepsilon)$ and other quantities in units according to Eqs. (6) and (7); $\varepsilon=0.004$.

VI. CONCLUSION

We have developed a time-dependent 2D discrete-variable approach for *ab initio* quantum-dynamical studies of atomic scattering processes in waveguides. Our wave-packet propagation techniques allow for the implementation of a finite-range atomic interaction, and in particular they provide a very natural approach to the dynamical as well as stationary properties of the scattering process. First we studied the case of scattering of two identical bosons that experience the same harmonic transversal confinement. We observed blocking of the transmission due to the confinement-induced resonance and derived the effective 1D coupling constant, which agrees very well with the analytical results predicted by zero-range s-wave interactions. Our second case study was that of two identical fermions, where the mapping onto free bosons in the resonant case was verified and the corresponding zero of the transmission of the wave packet was observed.

Employing our wave-packet propagation scheme, we analyzed the case of distinguishable atomic species scattering in a waveguide with different harmonic confinement for the different species. The latter leads to a coupling of the center-of-mass and relative motions of the atoms and also to a mixing of the different partial waves involved in the scattering process. We explored the important case of confined scattering with the ingredient that the corresponding 3D free scattering involves both s- and p-wave near-resonant behavior. We found that the interplay between the free-space s- and p-wave resonant scattering states due to the confinement leads to complete transmission in the scattering process: the so-called dual CIR. The dual CIR occurs due to a destructive

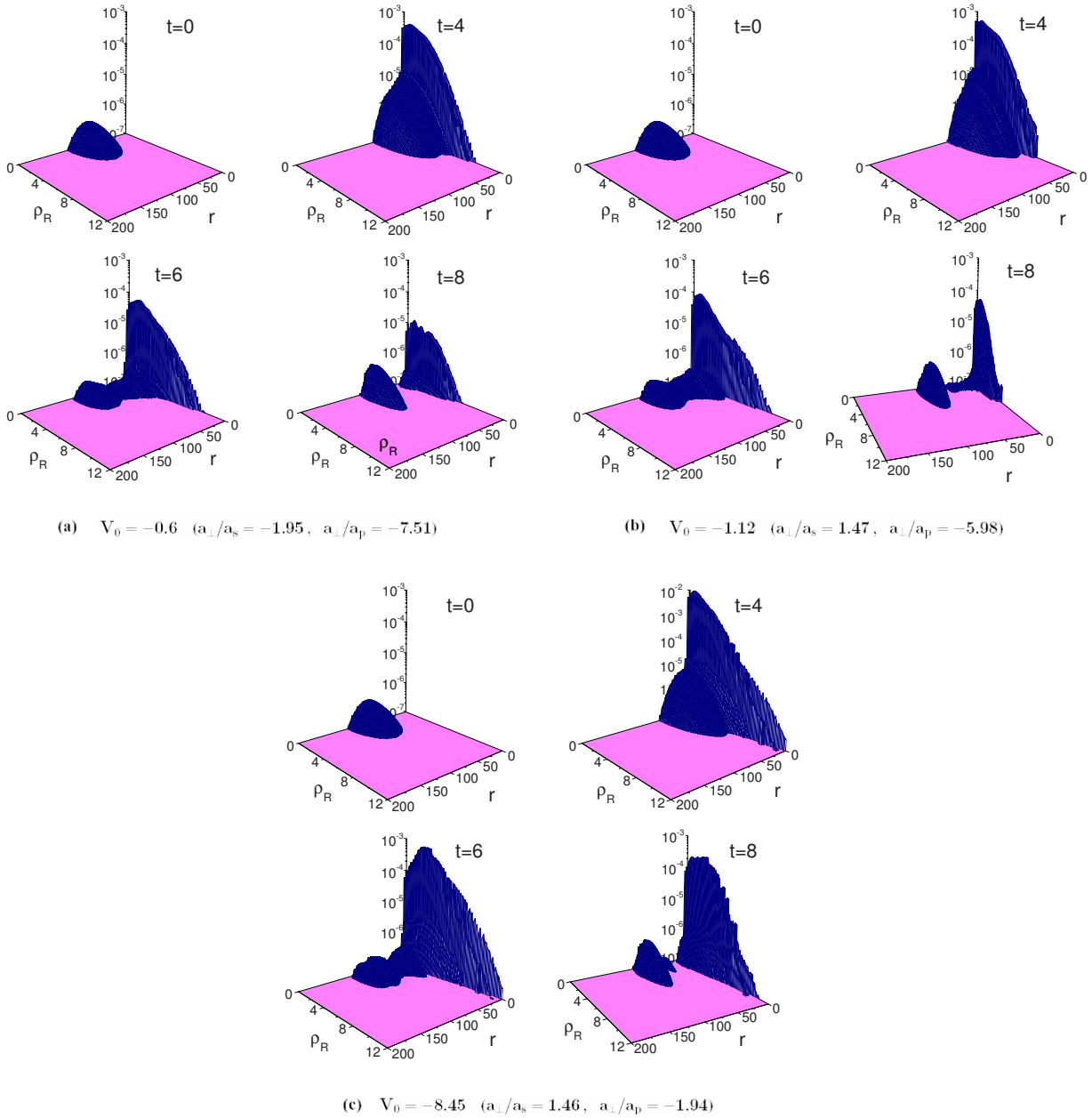

FIG. 8. (Color online) Time evolution of the probability density distribution in the harmonic trap $\omega_1/1.35=\omega_2=0.02$ averaged over the angular variables $W(\rho_R,r,t)=\int|\psi(\rho_R,r,\theta,\phi,t)/|^2(r^2\rho_R)\sin\theta\, d\theta\, d\phi$ for two distinguishable particles $m_1/m_2=40/87$ for the same three cases as in Fig. 7: (a) nonresonant free-space scattering $V_0=-0.6$; (b) s-wave resonant scattering in free space for $V_0=-1.12$ (creating a CIR in a harmonic trap); (c) simultaneous s- and p-wave resonant behavior in free space for $V_0=-8.45$ (creating a dual CIR in a harmonic trap). Time t is given in units of $t_0=2\pi/(\omega+\varepsilon)$ and other quantities in units according to Eqs. (6) and (7); $\varepsilon=0.004$.

interference between the s and p scattering waves in the quasi-1D waveguide.

In the future, our wave-packet dynamical approach will be employed to investigate quantum dynamics using realistic molecular potentials for the atomic scattering. The most promising candidates for new scattering properties are potentials with a rich spectral structure. The anharmonicity effects of the transversal confinement in the waveguide represent a further challenging perspective to be explored in a forthcoming study.

ACKNOWLEDGMENTS

V.S.M. acknowledges financial support in the framework of a visit to the University of Heidelberg by the Landesstiftung Baden-Württemberg, specifically the project "Mesoscopics and Atom Optics of Small Ensembles of Ultracold Atoms." Financial support by the Deutsche Forschungsgemeinschaft is gratefully acknowledged within Project No. Schm885/12-1. P.S. and V.S.M. acknowledge partial financial support by the Heisenberg-Landau Program through Grant No. HLP-2007/21.

[1] M. Lewenstein *et al.*, Adv. Phys. **56**, 243 (2007).
[2] R. Folman *et al.*, Adv. At., Mol., Opt. Phys. **48**, 263 (2002); J. Reichel, Appl. Phys. B: Lasers Opt. **74**, 469 (2002); J. Fortagh *et al.*, Rev. Mod. Phys. **79**, 235 (2007).
[3] M. Olshanii, Phys. Rev. Lett. **81**, 938 (1998).
[4] M. Girardeau, J. Math. Phys. **1**, 516 (1960).
[5] H. G. Vaidya and C. A. Tracy, Phys. Rev. Lett. **42**, 3 (1979); A. Minguzzi, P. Vignolo, and M. P. Tosi, Phys. Lett. A **294**, 222 (2002); M. D. Girardeau, E. M. Wright, and J. M. Triscari, Phys. Rev. A **63**, 033601 (2001); T. Papenbrock, *ibid.* **67**, 041601(R) (2003).
[6] T. Kinoshita, T. Wenger, and D. S. Weiss, Science **305**, 1125 (2004); B. Paredes *et al.*, Nature (London) **429**, 277 (2004).
[7] K. Günter, T. Stoferle, H. Moritz, M. Kohl, and T. Esslinger, Phys. Rev. Lett. **95**, 230401 (2005).
[8] T. Bergeman, M. G. Moore, and M. Olshanii, Phys. Rev. Lett. **91**, 163201 (2003).
[9] M. G. Moore, T. Bergeman, and M. Olshanii, J. Phys. IV **116**, 69 (2004).
[10] B. E. Granger and D. Blume, Phys. Rev. Lett. **92**, 133202 (2004).
[11] J. I. Kim, J. Schmiedmayer, and P. Schmelcher, Phys. Rev. A **72**, 042711 (2005).
[12] V. Peano, M. Thorwart, C. Mora, and R. Egger, New J. Phys. **7**, 192 (2005).
[13] J. I. Kim, V. S. Melezhik, and P. Schmelcher, Phys. Rev. Lett. **97**, 193203 (2006).
[14] J. I. Kim, V. S. Melezhik, and P. Schmelcher, Prog. Theor. Phys. Suppl. **166**, 159 (2007).
[15] H. Bock, I. Lesanovsky, and P. Schmelcher, J. Phys. B **38**, 893 (2005).
[16] V. S. Melezhik, Phys. Lett. A **230**, 203 (1997); *Atoms and Molecules in Strong External Fields*, edited by P. Schmelcher and W. Schweizer (Plenum, New York, 1998), p. 89; V. S. Melezhik and P. Schmelcher, Phys. Rev. A **59**, 4264 (1999); Phys. Rev. Lett. **84**, 1870 (2000); V. S. Melezhik and D. Baye, Phys. Rev. C **59**, 3232 (1999); **64**, 054612 (2001); P. Capel, D. Baye, and V. S. Melezhik, *ibid.* **68**, 014612 (2003); V. S. Melezhik, J. S. Cohen, and Chi-Yu Hu, Phys. Rev. A **69**, 032709 (2004).
[17] V. S. Melezhik and Chi-Yu Hu, Phys. Rev. Lett. **90**, 083202 (2003).
[18] J. V. Lill, G. A. Parker, and J. C. Light, Chem. Phys. Lett. **89**, 483 (1982); J. C. Light and T. Carrington, Jr., Adv. Chem. Phys. **114**, 263 (2000).
[19] D. Baye, J. Phys. B **28**, 4399 (1995).
[20] G. I. Marchuk, *Methods of Numerical Mathematics* (Springer-Verlag, New York, 1975), Sec. 4.3.3.
[21] V. de Alfaro and T. Regge, *Potential Scattering* (North-Holland, Amsterdam, 1965), Sec. 6.
[22] E. W. Schmid and H. Ziegelmann, *The Quantum Mechanical Three-Body Problem* (Pergamon Press/Friedrich Vieweg and Sohn, Braunschweig, 1974).
[23] M. D. Girardeau and E. M. Wright, Phys. Rev. Lett. **95**, 010406 (2005).